

Ultradispersed Palladium Nanoparticles in Three-Dimensional Dendritic Mesoporous Silica Nanospheres: Toward Active and Stable Heterogeneous Catalysts

Dengke Shen,[†] Lei Chen,[†] Jianping Yang,^{†,‡} Renyuan Zhang,[†] Yong Wei,[†] Xiaomin Li,[†] Wei Li,[†] Zhenkun Sun,[†] Hongwei Zhu,[†] Aboubakr M. Abdullah,[§] Abdullah Al-Enizi,[‡] Ahmed A. Elzatahry,[†] Fan Zhang,[†] and Dongyuan Zhao^{*,†}

[†]Department of Chemistry, Shanghai Key Laboratory of Molecular Catalysis and Innovative Materials, State Key Laboratory of Molecular Engineering of Polymers and Laboratory of Advanced Materials, Fudan University, Shanghai 200433, People's Republic of China

[‡]College of Environmental Science and Engineering, State Key Laboratory of Pollution Control and Resources Reuse, Tongji University, Shanghai 200092, People's Republic of China

[§]Center for Advanced Materials, Qatar University, Doha 2713, Qatar

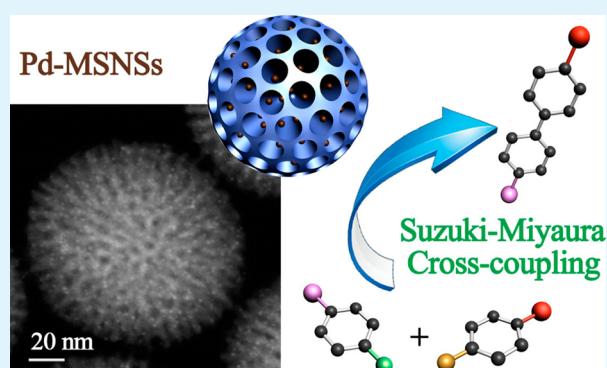
[⊥]Department of Chemistry, College of Science, King Saud University, Riyadh 11451, Saudi Arabia

^{||}Materials Science and Technology Program, College of Arts and Sciences, Qatar University, P.O. Box 2713, Doha, Qatar

Supporting Information

ABSTRACT: Immobilization of highly monodispersed palladium nanoparticles in colloidal mesoporous silica supports has been successfully achieved. The Pd nanoparticles with a uniform small size of ~1.2 nm can be homogeneously distributed in individual mesopore channels of amino group-functionalized three-dimensional dendritic mesoporous silica nanospheres (3D-dendritic MSNSs) with a Pd content of ~2.8%. The 3D-dendritic MSNSs-based nanoreactors show high activity in Suzuki–Miyaura cross-coupling reactions of bromobenzene with phenylboronic acid, obtaining a yield over 99% with 0.075 mol % Pd catalyst at room temperature in the dark within 12 h. More importantly, the excellent catalytic performance can be maintained with a negligible decrease lasting at least six cycles. It further reveals that the mesoporous frameworks of the colloidal silica supports can be well-preserved after four catalytic runs; meanwhile, the Pd nanoparticles in the mesopore channels also can remain the sizes of 1.5 ± 0.3 nm without significant transfer and aggregation. The unique mesostructure of the 3D-dendritic MSNSs with mesopore channels of short length and large diameter is supposed to be the key role in immobilization of active and robust heterogeneous catalysts, and it would have more hopeful prospects in catalytic applications.

KEYWORDS: mesoporous silica, colloidal nanospheres, palladium, nanosupports, heterogeneous catalysts



INTRODUCTION

Because of the rapid progress of nanoscience and nanotechnology, immobilization of catalytic active components onto solid supports not only provides a way to improve stability and reusability but also can modify the catalytic properties, even getting high activity or selectivity in certain cases.^{1–6} The novel nanostructured support materials can be used in the preparation of heterogeneous catalysts to maximize the surface area of the active phase.^{7–10} Among nanostructured supports, porous materials show their unique advantages against others, because of the tunable pore sizes, high surface area and large pore volume.^{11–14} Particularly, mesopore channels of the supports can provide a confined nanospace for preventing aggregation of metal catalysts.^{15,16}

However, classic surfactant-templated mesoporous solid supports possessing isolated channels with excessive length to afford inefficient in-pore diffusion of substrates, resulting in poor catalytic turnover.^{17–19} A typical example is ordered mesoporous silica SBA-15, which has micrometer-sized bulk morphology with the mesostructure of micrometer-long and parallel mesopore channels, and the high surface area even leads to the low in-pore molecule diffusion and the high nonspecific adsorption.^{20,21} Because of the inefficient mass-transport and poor pore accessibility of the conventional mesostructures, it is

Received: June 7, 2015

Accepted: July 20, 2015

Published: July 20, 2015

still a major challenge to immobilize catalysts with homogeneous distribution in an individual pore channel of the mesoporous support materials,^{15,22} leaving a large amount of blank pore channels to be nonconductive to catalytic turnover efficiency. Moreover, the mesopore channels are usually used as the confined nanospaces in the *in situ* growth process, obtaining catalyst nanoparticles with the same size to pore diameter and plugging the pore channels to reduce the effective specific surface area. Unfortunately, it is still difficult to control the catalytic active nanoparticles with small sizes, especially <2 nm, regardless of whether via an *in situ* growth or a postloading approach.^{15,23,24} Thus, further improvement of mesostructures is hence required to optimize mass-transport of reactants and pore channel accessibility.

Shortening the length of mesopore channels is an effective way to improve the mass-transport of the porous support materials, and various monodispersed core-shell or yolk-shell nanoreactors have been designed and achieved, which have catalytic active materials as a core and mesopore channels with controlled length as a shell.^{25–28} Unfortunately, in the monodispersed nanoreactor system, the mesopore channels lose their function as the supports due to the small pore size in the previous reports. The hollow structure formed with mesoporous shells provides a confined nanospace to prevent from aggregation of catalytic active components in different nanoreactors. However, in a single nanoreactor, the size of catalyst nanoparticles is difficult to be very small, leading to the few and limited exposed catalytic active sites.^{29,30} To achieve immobilization of catalyst nanoparticles in the pore channels without blocking, the colloidal mesoporous nanoparticles with large pores and stable framework are desired.

Recently, we have developed an efficient biphasic stratification approach to synthesize three-dimensional dendritic mesoporous silica nanospheres (3D-dendritic MSNSs) with large center-radial mesopore channels,³¹ providing numerous opportunities for preparation of novel and functional mesoporous silica-based composites. Herein, we demonstrate that 3D-dendritic MSNSs can be used as a desired good catalyst support, because they not only have ideal monodispersity with nanospherical morphology but also have a dendritic-like unique mesostructure with tunable pore diameter and channel length. Immobilization of ultradispersed palladium nanoparticles in amino group-functionalized 3D-dendritic MSNSs was successfully achieved via *in situ* growth strategy, and the distribution of precious metal (Pd) in the mesopore channels of the colloidal nanosupports was very homogeneous with a particle size of ~1.2 nm. To the best of our knowledge, this is the first time to report the immobilization of palladium nanoparticles in colloidal mesoporous supports with homogeneous high-dispersity and small size. The Suzuki–Miyaura reaction has been selected as a model for evaluating 3D-dendritic MSNSs-based nanoreactors, and the immobilized palladium catalysts showed the active and stable heterogeneous catalytic performance.

EXPERIMENTAL SECTION

Chemicals. Cetyltrimethylammonium chloride (CTAC) solution (25 wt % in H₂O), triethanolamine (TEA) and 3-aminopropyltriethoxysilane were purchased from Sigma-Aldrich (UK). Tetraethyl orthosilicate (TEOS) and potassium hexachloropalladate (IV) (K₂PdCl₆) were purchased from Aladdin Reagent Co., Ltd. All other reagents were purchased from Sinopharm Chemical Reagent Co., Ltd.

(analytical reagent grade). All chemicals were used as received without purification.

Preparation of Three-Dimensional Mesoporous Silica Nanospheres. The 3D-dendritic mesoporous silica nanospheres (3D-dendritic MSNSs) with particle size of ~125 nm and pore size of ~6 nm were achieved via the biphasic stratification approach as reported with a little modification.³¹ A typical synthesis of the 3D-dendritic MSNSs was performed as following. At first, 48 mL of (25 wt %) CTAC solution and 0.36 g of TEA were added to 72 mL of water and stirred gently at 60 °C for 1 h in a 250 mL round-bottomed flask, then 40 mL of (20 v/v %) TEOS in cyclohexane was carefully added to the water–CTAC–TEA solution, and the mixture was kept at 60 °C in an oil bath under magnetic stirring. A standard Teflon-coated stirring bar with a length of 3 cm was employed, and the stirring rate was set to be very slow, to avoid mixing of the phases. The reaction was then kept at 60 °C for 12 h, and the upper oil was removed carefully. The temperature was then elevated to 90 °C for ripening, and after 3 h the products were collected by centrifugation and washed for several times with ethanol to remove the residual reactants. Then, the collected products were extracted with a 0.6 wt % ammonium nitrate (NH₄NO₃) ethanol solution at 60 °C for 18 h twice to remove the template. The extracted 3D-dendritic MSNS products were lyophilized to obtain the dry powder for next experiments.

Preparation of Amino-MSNSs. The amino-functional 3D-dendritic MSNSs (amino-MSNSs) were achieved via a postgrafting strategy. In a typical process, 15 mL of anhydrous toluene and 400 mg of extracted 3D-dendritic MSNS dry powder was mixed in a 25 mL round-bottomed flask and stirred vigorously. After formation of a homogeneous suspension, 1.0 mL of 3-aminopropyltriethoxysilane was carefully added to toluene solution of extracted 3D-dendritic MSNSs. The reaction was kept at 110 °C with reflux for 20 h. The amino-functional products were collected by centrifugation and washed for several times with ethanol to remove the residual reactants and subsequently lyophilized to obtain the dry powder for the next experiments.

Preparation of Pd-MSNSs. Immobilization of palladium nanoparticles in the mesopore channels was achieved via *in situ* growth approach. In a typical process, 56 mg of amino-MSNSs was dispersed in 10 mL of deionized water via sonication. After the mixture was stirred for 15 min at 30 °C, 6.0 mL of fresh K₂PdCl₆ aqueous solution with a concentration of 1.0 mg/mL was added dropwise and kept at 30 °C with stirring for 4 h. Then 1.0 mL of 0.1 M NaBH₄ solution was added dropwise, and the mixture was aged at the same temperature for 24 h. The palladium-loaded products were separated by centrifugation, washed with water and ethanol, and dried at 60 °C. The dried products can be stored in the anoxic environment, and they can be stable for several months. They can be used directly as the catalysts. For different palladium-immobilized amino-MSNSs, samples were prepared by a similar method at different temperatures.

Suzuki–Miyaura Cross-Coupling Reactions. Typically, aryl halide (0.5 mmol), phenylboronic acid (1 mmol), K₂CO₃ (0.14 g, 1.0 mmol), a certain amount of palladium-containing catalysts and 6.0 mL of methanol were added to a 25 mL round-bottomed flask, and the reaction mixture was stirred vigorously at 30 °C in the darkness. At certain periods, the palladium-containing catalysts were separated by centrifugation, then the solvent was removed by rotary evaporator. The crude product was dissolved by CHCl₃, and directly used for measurements by analyzed gas chromatography–mass spectrometer (GC–MS), using a PerkinElmer clarus 680-SQ8T equipped with a PE-SMS capillary column.

Characterization and Measurements. Nitrogen adsorption–desorption measurements were conducted to obtain information on the porosity. The measurements were conducted at 77 K with a Micromeritics Tristar 3020 analyzer (USA). The Brunauer–Emmett–Teller (BET) specific surface area (A_{BET}) was calculated from the adsorption data in the relative pressure (P/P_0) ranging from 0.04 to 0.1. The pore size (D_p) distribution was calculated from the adsorption branch of the isotherms using the Barrett–Joyner–Halenda (BJH) formula. Transmission electron microscopy (TEM), high angle annular dark field imaging in the scanning TEM (HAADF-

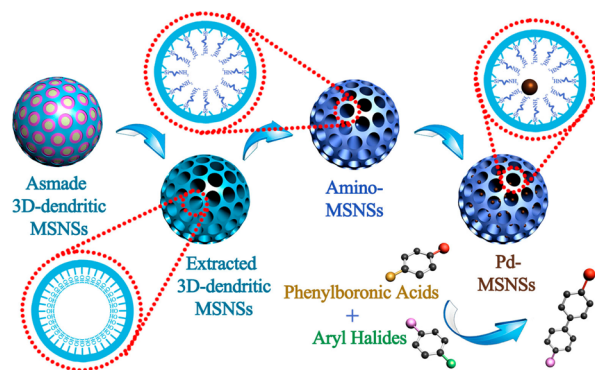
STEM) and energy dispersive spectroscopy (EDS) observations were performed on JEM-2100F transmission electron microscope with an accelerating voltage of 200 kV equipped with a postcolumn Gatan imaging filter (GIF-Tridium). For TEM measurements, the samples were dispersed in ethanol and then dried on a holey carbon film Cu grid. Small-angle X-ray scattering (SAXS) measurements were taken on a Nanostar U small-angle X-ray scattering system (Bruker, Germany) using Cu K α radiation (40 kV, 35 mA). The d -spacing values were calculated by the formula $d = 2\pi/q$, wherein q is the scattering vector. Fourier-transform infrared (FTIR) spectra were recorded on a Nicolet Magna-IR 550II spectrophotometer using KBr pellets. The metal content in the Pd-MSNSs sample were measured by using inductively coupled plasma-atomic emission spectrometry (ICP-AES, Varian VISTA-MPX).

RESULTS AND DISCUSSION

The 3D-dendritic MSNSs were prepared in a heterogeneous oil–water biphasic stratification reaction system according to the method reported previously in our group.³¹ The upper oil phase was cyclohexane solution of tetraethyl orthosilicate (TEOS) and the lower aqueous phase was the solution combined by cationic cetyltrimethylammonium chloride (CTAC) and triethanolamine (TEA). After undergoing a hydrothermal aging, the obtained mesoporous silica colloidal products displayed good monodispersity and stability in ethanol and toluene for several months, or in aqueous solution with weak base for several weeks.

The amino-function of 3D-dendritic MSNSs have been successfully achieved via an extracting and postgrafting approach (Scheme 1), and the products are named as extracted

Scheme 1. Synthesis and Catalytic Process of Highly Monodispersed Palladium Nanoparticles Immobilized in Three-Dimensional Dendritic Mesoporous Silica Nanospheres for Suzuki–Miyaura Cross-Coupling Reaction



3D-dendritic MSNSs and amino-MSNSs, respectively. The whole process of the surfactant removal and functionalization of amino group was tracked by Fourier-transform infrared (FTIR) spectra (Figure S1a). The disappearance of the strong absorption bands around 2920 and 2849 cm^{-1} can be observed after the reflux of the as-made 3D-dendritic MSNSs in ammonium nitrate ethanol solution for 36 h (Figure S1a, blue and black lines), demonstrating that the surfactant templates are removed via the solvent extraction. The absorption band at $\sim 1530 \text{ cm}^{-1}$ can be observed after toluene reflux with 3-aminopropyltrimethoxysilane, illuminating that the amino groups are successfully modified. The transmission electron microscopy (TEM) images show that the mesoporous silica colloidal nanospheres retain a uniform particle size of $\sim 125 \text{ nm}$ before and after grafting the amino groups (Figure

S1b and Figure 1a). The center-radial mesopore channels with a diameter of $\sim 6 \text{ nm}$ are evident, and no significant change can be observed in the mesostructure during the grafting process. According to the nitrogen adsorption–desorption isotherms, a capillary condensation step can be clearly observed at around $0.4 < P/P_0 < 0.7$ for the sample extracted 3D-dendritic MSNSs (Figure S1c, black line). And a little low-pressure shift can be observed for the sample amino-MSNSs (Figure S1c, red line), providing a clear evidence for the decrease of pore size after the amino grafting and retaining a narrow diameter distribution. The BET surface area is measured to be ~ 406 and $\sim 302 \text{ m}^2 \text{ g}^{-1}$ before and after the modification of amino group. Using the Barrett–Joyner–Halenda (BJH) model, the total pore volume and pore size distributions of the sample extracted 3D-dendritic MSNSs are estimated to be $\sim 1.03 \text{ cm}^3 \text{ g}^{-1}$ and $\sim 6 \text{ nm}$, respectively (Figure S1d, black line). And for the sample amino-MSNSs, they decrease to $\sim 0.73 \text{ cm}^3 \text{ g}^{-1}$ and $\sim 5.4 \text{ nm}$, respectively (Figure S1d, red line). In addition, SAXS patterns show that a single scattering peak at $\sim 0.73 \text{ nm}^{-1}$ can be observed before and after functionalization of amino group, suggesting that the uniform mesostructure can be well retained (Figure S1e). All these results further confirm that the amino groups can be grafted homogeneously on the inner silica wall surface of the mesopore channels of 3D-dendritic MSNSs with the well-preserved mesostructure.

Immobilization of palladium nanoparticles in the mesopore channels of amino-MSNSs was achieved via the *in situ* growth strategy, which was a process of a reaction with the precursor (K_2PdCl_6) first and a complete reduction with NaBH_4 later (Scheme 1). The obtained products are named as Pd-MSNSs-30, when reaction temperature is $30 \text{ }^\circ\text{C}$. Pd-MSNSs-30 can be well dispersed in water, showing the pellucid colloidal solution with dark brown color (Figure S2b). The representative TEM image of as-made Pd-MSNSs-30 shows almost the same samples to blank amino-MSNSs (Figure 1a,b). No palladium nanoparticles can be observed distinctly, even in a large magnification and defocused view (Figure 1c,d). However, Pd content of the sample Pd-MSNSs-30 is measured by inductively coupled plasma atomic emission spectroscopy (ICP-AES) to be $\sim 2.8\%$, consistent with the calculated content. Meanwhile, energy dispersive spectroscopy (EDS) analysis of the sample indicates Pd/Si atomic ratio of $\sim 2:98$ (Figure 1e), also corresponding to the amount of Pd precursors and silica supports. These results obviously suggest that Pd catalysts are successfully loaded into the mesoporous silica supports, but they are difficult to be observed in TEM images. High-angle annular dark-field scanning TEM (HAADF-STEM) is a powerful technique to distinguish local chemical information with different atomic numbers, and in the HAADF-STEM image at the same observation domain (Figure 1f corresponding bright-field image of Figure 1b), some bright spots are very clear with an obvious contrast with the amino-MSNSs, suggesting that the palladium nanoparticles are existent with a very small size. In the HAADF-STEM image at a large magnification, the dispersion of bright spots is not only even in the whole of the amino-MSNSs (Figure 1g) but also uniform along the walls of center-radial mesopore channels (Figure 1h), demonstrating a homogeneous distribution of ultradispersed palladium nanoparticles. The size distribution of Pd nanoparticles in Pd-MSNSs-30 estimated from the HAADF-STEM image (Figure 1h) has a typical Gaussian shape, where the average diameter of Pd nanoparticles is about 1.2 nm with a narrow dispersion of 0.1 nm (Figure 1i). The Pd 3d XPS

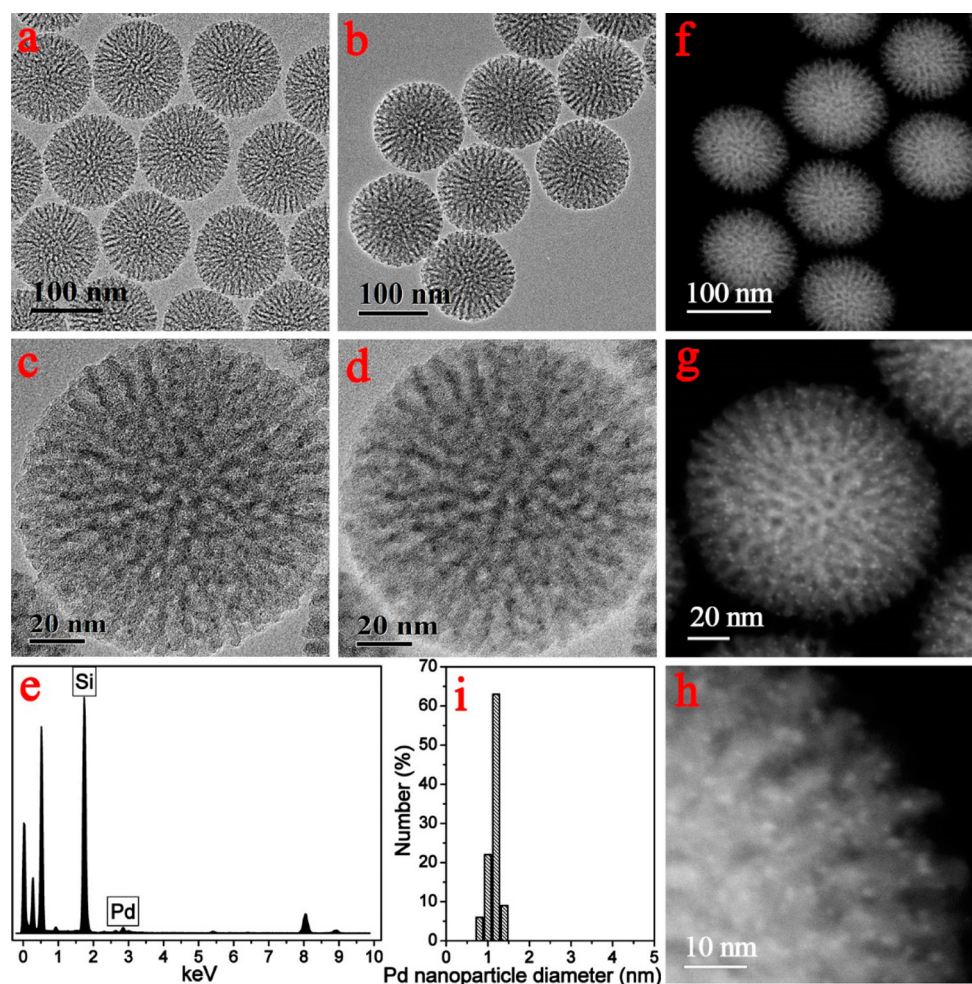


Figure 1. TEM images of the amino-MSNSs (a); TEM images (b, c, d), EDS analysis (e) and HAADF-STEM images (f, g, h) of Pd-MSNSs-30 prepared via the *in situ* growth approach; size distribution of palladium nanoparticles in Pd-MSNSs-30 (i).

spectroscopy (Figure S4b) demonstrates that about 76% of palladium is in metallic form (Pd^0), as revealed by Pd $3d_{3/2}$ and Pd $3d_{5/2}$ XPS peaks centered at 340.3 and 335.0 eV, respectively.³² In addition, no evident Pd-corresponding scattering peaks can be observed in the XRD pattern, because of the small particle size of immobilized palladium nanoparticles.

To investigate the role of reaction temperature in *in situ* growth approach to palladium nanoparticles, a series of products were obtained at 10, 50, or 70 °C, and they were named as Pd-MSNSs-10, Pd-MSNSs-50 and Pd-MSNSs-70, respectively. In the bright-field TEM images of the sample Pd-MSNSs-50 with different magnifications and focused/defocused view, palladium nanoparticles are very difficult to be identified. Similarly, in the HAADF-STEM images at the corresponding viewing zone, the ultradispersed bright spots are exhibited with all different magnifications, providing evidence for homogeneous distribution of palladium nanoparticles in the sample amino-MSNSs. However, the mean diameter of palladium nanoparticles is estimated from the HAADF-STEM images to be 1.3 ± 0.2 nm (Figure 2f), suggesting that the nanoparticles grown in 50 °C are not as uniform as ones in 30 °C. ICP-AES results reveal that the Pd content of sample Pd-MSNSs-50 is $\sim 2.8\%$, and the atomic ratio of palladium and silicon in the sample is semiquantitated to be $\sim 2:98$ by EDS analyses (Figure 2g). The Pd 3d XPS spectroscopy reveals that

about 77% palladium is metallic form (Pd^0) (Figure S4c). When the reaction temperature is changed to 10 or 70 °C, the products Pd-MSNSs-10 and Pd-MSNSs-70 both have a small amount of Pd nanoparticles with the diameter larger than 5 nm, which are distinct in both bright-field TEM images and HAADF-STEM images (Figure S3). The above results indicate that uniform sizes of palladium nanoparticles are mainly depended on the *in situ* growth temperature.

The *in situ* growth of palladium nanoparticles in the amino-MSNSs is divided into two steps: a weak reduced nucleation and a strong growth. The key factor in the formation of the ultradispersed Pd nanoparticles with a small size is supposed to be the homogeneous weak reduced nucleation, which is a process mainly depended on the amino groups in amino-MSNSs. The amino groups on the inner surface of the mesopore channels not only can coordinate with PdCl_6^{2-} but also have reducibility to metal precursors.³⁰ The reduction capability of the amino groups can be enhanced with the increase of reaction temperature; meanwhile, the coordination effect of them can effectively inhibit the violent self-hydrolysis reaction of Pd precursors and moderate nucleation process. Therefore, the coordination and reduction effects can be regulated via a suitable reaction temperature to cooperate optimally, such as 30 °C, leading to the homogeneous weak reduced nucleation, and finally formation of the palladium nanoparticles with uniform size by a NaBH_4 reduction.

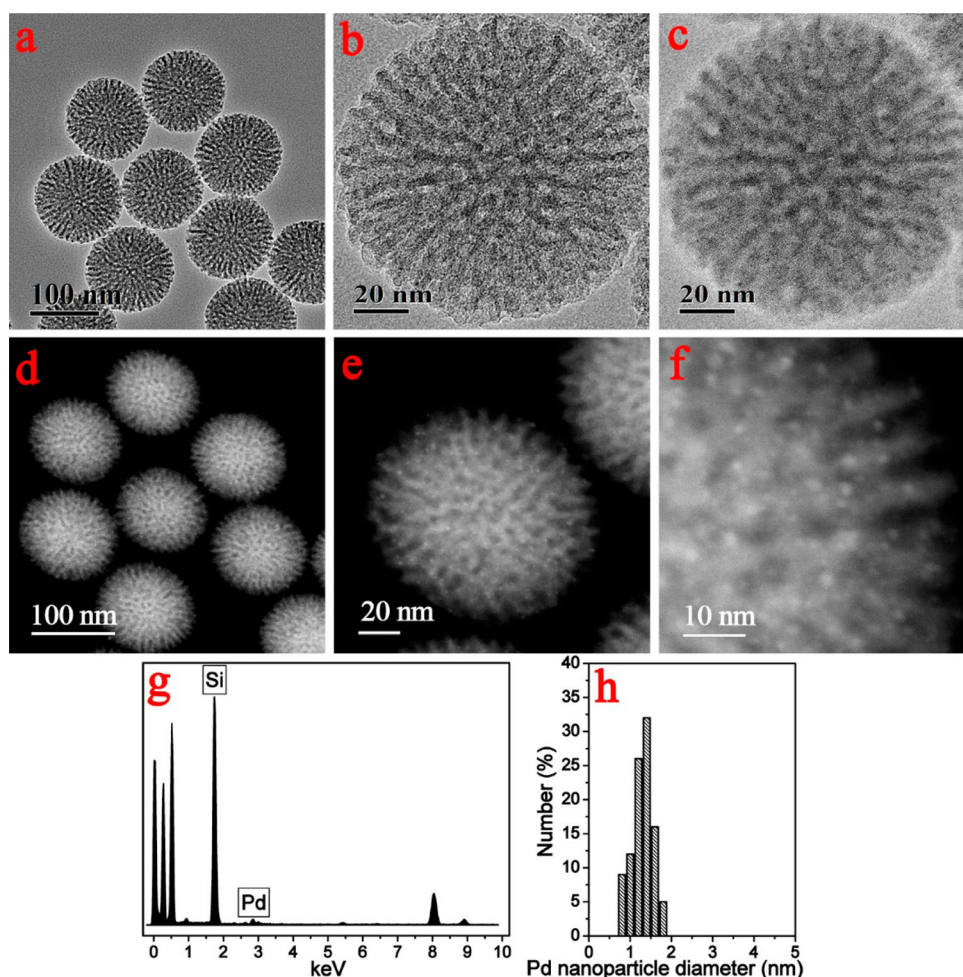


Figure 2. TEM images (a, b, c), HAADF-STEM images (d, e, f) and EDS analysis (g) of the sample Pd-MSNSs-50 prepared via the *in situ* growth approach; size distribution of palladium nanoparticles in the sample Pd-MSNSs-50 (h).

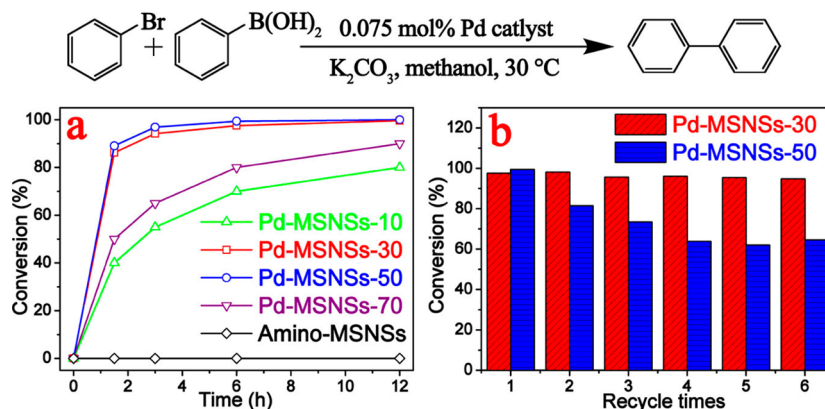


Figure 3. Catalyst screening (a) in the Suzuki–Miyaura reaction coupling of bromobenzene and phenylboronic acid with the samples Pd-MSNSs-10 (green), Pd-MSNSs-30 (red), Pd-MSNSs-50 (blue), Pd-MSNSs-70 (purple) and blank supports (3D-dendritic-MSNSs without Pd) as the control (black); the chart of yield correlating with the number of reuse cycles (b) using the Pd-MSNSs-30 (red) and Pd-MSNSs-50 (blue) as a catalyst for coupling of bromobenzene and phenylboronic acid. Reactions were carried out with bromobenzene (0.5 mmol), phenylboronic acid (1.0 mmol), K_2CO_3 (1.0 mmol), methanol (6 mL) and the Pd catalyst of 0.075 mol % at room temperature (30 °C) under atmospheric conditions in the dark. The conversion and yield were determined by gas chromatography mass spectrometry (GC–MS) analysis using tetradecane as the internal standard.

Accordingly, the presence of some large and isolated Pd nanoparticles in the samples Pd-MSNSs-10 and Pd-MSNSs-70 also conform to the above formation process. At the low temperature of 10 °C, the amino groups-induced reduced nucleation is limited and inhomogeneous because coordination

is the major reaction, leading to the aggregated nanoparticles when violent reduction of Pd precursors; whereas at a high temperature such as 70 °C, the reducibility of the amino groups become dominant and the nucleation is drastic and uneven, obtaining the final products with nonuniform Pd nanoparticles

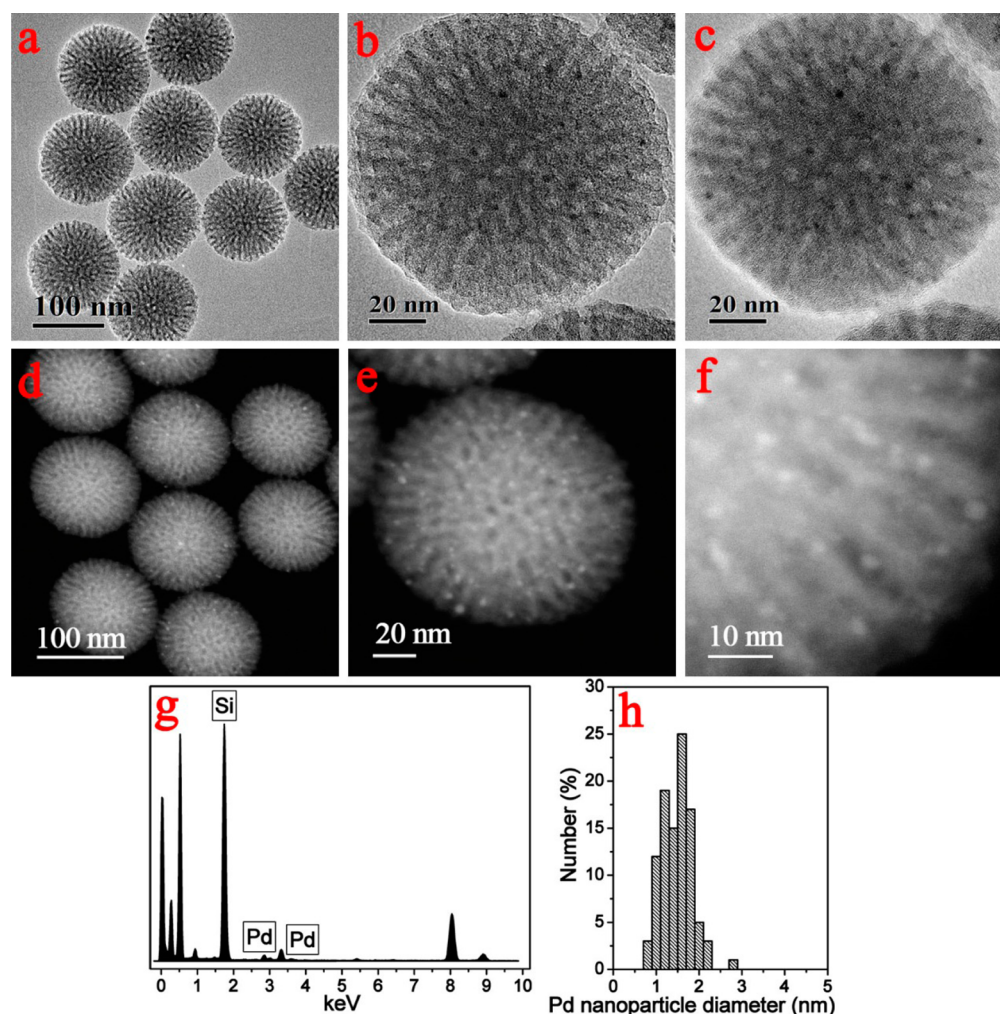


Figure 4. TEM images (a, b, c), HAADF-STEM images (d, e, f) and EDS analysis (g) of the sample Pd-MSNSs-30 after four catalytic cycles; size distribution of palladium nanoparticles in the corresponding sample (h).

inheriting from inhomogeneous nucleuses. In addition, the *in situ* growth approach can also immobilize other kinds of noble metal in 3D-dendritic MSNSs, such as Au (Figure S5), suggesting that it can be considered as the general desired nanosupports for metal nanoparticles.

Suzuki–Miyaura cross-coupling reaction was chosen as a model catalytic reaction (Scheme 1), and four types of palladium-immobilized 3D-dendritic MSNSs with an identical loading amount of palladium but different particle sizes were employed as the nanoreactors to catalyze the bromobenzene and phenylboronic acid C–C coupling reaction to evaluate the size-dependent catalytic activity. As shown in Figure 3a, it is clear that the conversion order is Pd-MSNSs-30 > Pd-MSNSs-50 > Pd-MSNSs-70 > Pd-MSNSs-10, and such results can be attributed to the different exposed surface areas of catalytic activated palladium. The sample Pd-MSNSs-30 has the highest catalytic activity among the four types of nanoreactors, obtaining a perfect conversion of over 99% with a Pd-catalyst as low as 0.075 mol %, because the Pd nanoparticles immobilized at 30 °C is the most ultradispersed and homogeneous with the smallest size among these four samples.

Furthermore, the recyclability of the samples Pd-MSNSs-30 and Pd-MSNSs-50 was also studied in the Suzuki–Miyaura cross-coupling reaction forming biphenyl. These two types of 3D-dendritic MSNSs-based nanoreactors have the approxi-

mated catalytic activity in the first run; nevertheless, the evident disparity between them can be revealed since the second run (Figure 3b). Reuse of the Pd-MSNSs-30 is accompanied by an excellent maintaining of activity in the second run (98.1% conversion) and a slight loss with 95.6% yield in the second run; contrastively, Pd-MSNSs-50 has a substantial decrease in activity in the second and following runs. The catalytic activity can be maintained approximately in the six runs for the sample Pd-MSNSs-30; however, Pd-MSNSs-50 continuously loses its activity in the next several cycles, leaving only 63.8% conversion in the fourth run.

To explain the performance in recycling experiments, the two types of 3D-dendritic MSNSs-based nanoreactors after being used for four runs were recovered and tracked by bright-field TEM and HAADF-STEM images. The mesostructure of the sample Pd-MSNSs-30 can be well retained after four catalytic cycles, revealing the stability of the silica supports tolerating the alkaline catalytic environment (Figure 4a,b). The immobilized palladium nanoparticles can retain their locations in the mesopore channels of 3D-dendritic MSNSs without significant transfer and aggregation (Figure 4b–e), and the particle size has a little increase with an average diameter of 1.5 ± 0.3 nm (Figure 4f,h), demonstrating the confinement effect of the nanospace to prevent Pd nanoparticles from the aggregation. ICP-AES analysis reveals that the Pd content of the sample Pd-

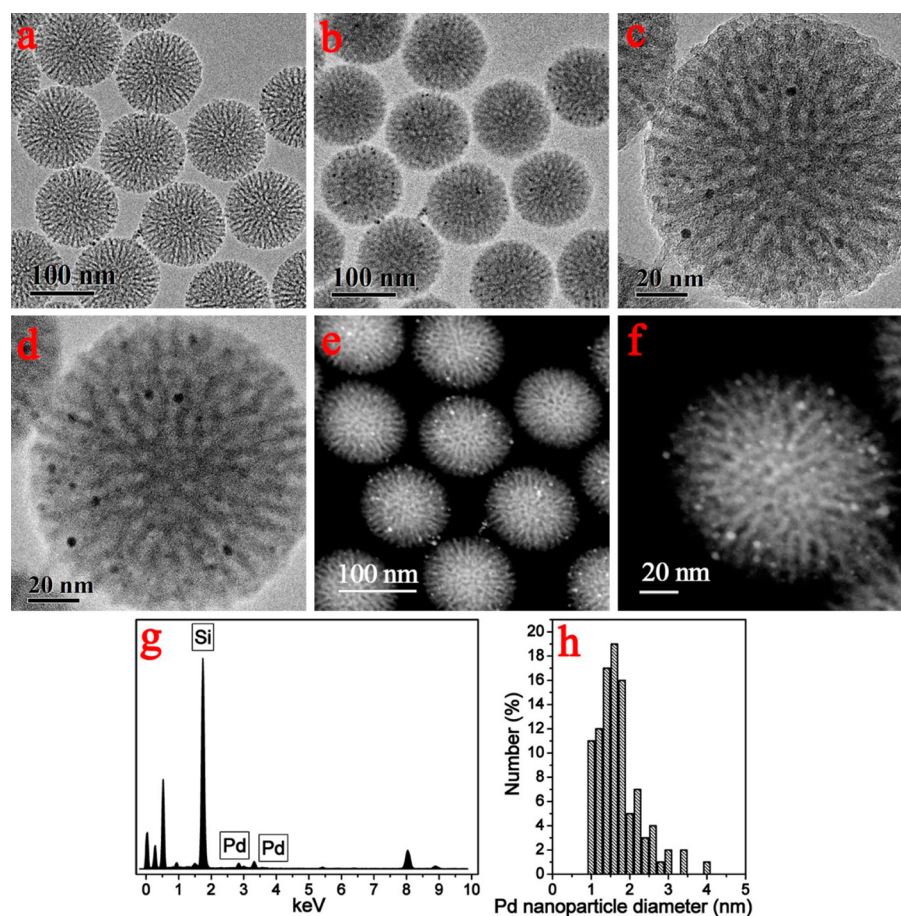


Figure 5. TEM images (a, b, c), HAADF-STEM images (d, e, f) and EDS analysis (g) of the sample Pd-MSNSs-50 after being reused for four catalytic cycles; the size distribution of palladium nanoparticles in the corresponding sample (h).

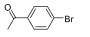
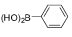
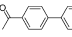
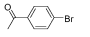
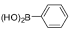
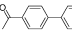
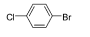
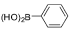
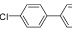
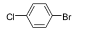
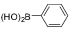
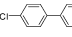
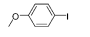
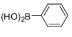
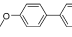
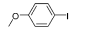
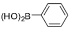
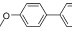
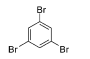
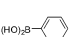
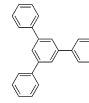
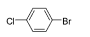
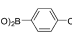
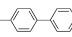
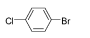
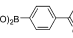
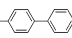
MSNSs-30 can remain $\sim 2.8\%$ after four cycles, showing imperceptible Pd leaching during the process. EDS analysis also proves that the atomic ratio of Pd/Si in Pd-MSNSs-30 is unchanged with 2:98 after four runs (Figure 4g), indicating that negligible wastage of noble metal occurs during the running. On the other hand, the mesopore channels of the sample Pd-MSNSs-50 also can be well retained after being used for four catalytic cycles, illustrating the stability of silica support frameworks (Figure 5a). However, in the defocused bright-field TEM image (Figure 5b) and HAADF-STEM image (Figure 5e) with the corresponding viewing zone (Figure 5a), some palladium nanoparticles with a large size (>3 nm) can be observed clearly, located in the opening of the mesopore channels. A representative HAADF-STEM image with a large magnification of the sample Pd-MSNSs-50 after being used for four runs reveals the heterogeneous distribution of Pd nanoparticles with nonuniform sizes of 1.7 ± 0.4 nm (Figure 5f). The Pd content of the sample Pd-MSNSs-50 after being reused for four cycles was measured by ICP-AES analysis to be $\sim 2.8\%$, and the atomic ratio of Pd/Si was $\sim 2:98$ based on the EDS analysis, clearly suggesting no significant loss of Pd during the catalytic processes. All above results suggest that the Pd nanoparticles grown at 30°C have better retainability of dispersity than the ones obtained in 50°C , leading to better reusability of the sample Pd-MSNSs-30 than Pd-MSNSs-50. The slight nonuniformity of Pd nanoparticles in the as-made Pd-MSNSs-50 is supposed to be the possible reason for the

presence of the ones with the growing size of supra-3 nm after the catalytic cycles.

An array of aryl halides and phenylboronic acids, whether electron-rich or electron-deficient, were chosen to be the substrate of Suzuki–Miyaura cross-coupling reaction for further investigation of the catalytic performance of the sample Pd-MSNSs-30. As illustrated in Table 1, more than 90% conversion of 4-bromoacetophenone or 1-bromo-4-chlorobenzene can be realized with Pd concentration of the catalyst as low as 0.075 mol % at room temperature within 6 h, and the presence of a little biphenyl in the catalytic products leads to a bit lower yield than the conversion. Using the Pd catalyst with 0.375 mol %, the conversion of these two types of electron-deficient aryl halides can reach over 99% at room temperature within 3 h. It also exhibits an excellent performance in the catalysis of 4-iodoanisole with a conversion of 99% within 12 h by the Pd catalyst with 0.75 mol %. For 1,3,5-tribromobenzene, the yield of 1,3,5-triphenylbenzene can be 84% at room temperature within 24 h, with 1% 1,3-dibromo-5-phenylbenzene and 1% 1-bromo-3,5-diphenylbenzene. In addition, 4-acetylphenylboronic acid and 4-methoxyphenylboronic acid were found to be relatively less effective substrates, as compared with the phenylboronic acids coupling with 1-bromo-4-chlorobenzene, revealing high conversions of 84% and 65% within 6 h, respectively.

It has been well documented that metal Pd^0 plays a primary role in Suzuki–Miyaura cross-coupling reaction.^{5,33–36} Although debate still surrounds the details of leaching-

Table 1. Results of Suzuki–Miyaura Cross-Coupling Reactions^a

Aryl halide	Phenylboronic acid	Product	Pd (mol %)	Time (h)	Conversion (%)	Yield (%)
			0.075	6	92	90
			0.375	3	> 99	96
			0.075	6	90	89
			0.375	3	> 99	97
			0.375	6	85	83
			0.75	12	99	96
			0.375	24	97	84
			0.375	6	84	65
			0.375	6	65	59

^aReactions were carried out with aryl halide (0.5 mmol), phenylboronic acid (1.0 mmol), K₂CO₃ (1.0 mmol), methanol (6.0 mL) and a certain amount of the Pd catalysts at room temperature (30 °C) under atmospheric conditions. The conversions and yields were determined by gas chromatography mass spectrometry (GC–MS) analysis using tetradecane as the internal standard.

redeposition mechanism in the catalytic cycle of heterogeneous catalysts, it is established that an amount of metals can go into solution as Pd⁰ atoms from the nanoparticle surface and catalyze the reaction, returning to the solid support after completion of the transformation.³⁷ Accordingly, there is a critical contradiction between leaching and redeposition. On one hand, several reports have provided detailed evidence to uncover the important role of leachable Pd⁰ atoms, demonstrating that efficient leaching can lead to the superior catalytic performance.³² On the other hand, the deactivation possibly owes to the less-controlled redeposition process of soluble Pd⁰ atoms on the solid support, which leads to the aggregated nanoparticles with lower surface and less leachable Pd⁰ atoms than before.³⁷ Consequently, high catalytic activity is based on Pd⁰ atoms with a low stability, high leaching susceptibility and large exposed surface, which tend to significant deactivation via vigorous and uncontrollable leaching–redeposition process. In this work, 3D-dendritic MSNS supports are employed as a nanoreactor, and the well-dispersed palladium nanoparticles with small size are immobilized in the mesopore channels with homogeneous distribution via an *in situ* approach. The naked metallic Pd nanoparticles can be suspended homogeneously in the catalytic reaction system, which is similar to the form of quasi-solution due to the colloidal mesoporous support with desired pore channel accessibility, revealing a superior catalytic performance. On one hand, although the size of Pd nanoparticles increases a little bit after several catalytic cycles, they can mainly retain a high activity and small size, suggesting that the unique mesostructure of 3D-dendritic MSNSs plays a key role in preventing Pd nanoparticles from aggregation. The unique mesostructure of 3D-dendritic MSNS supports is supposed to be the key role in reconciling the contradiction between efficient leaching and restrained redeposition of metal catalysts, because the mesopore channels with short length and large

diameter provide the individual quasi-confined nanospaces with promoted mass-transport and accessibility of reactants, achieving the immobilized catalysts with activity and robust stability at the same time. One the other hand, the mesostructure of 3D-dendritic MSNSs cannot prevent the Pd nanoparticles in the same pore channel from aggregation. The slight sizes, nonuniformity and distributional inhomogeneity of Pd nanoparticles in the as-made samples can be significantly enlarged after the cyclic catalysis, and some overgrown Pd nanoparticles can be observed, resulting in the fast loss of catalytic activity. Therefore, the homogeneous distribution of Pd nanoparticles in nanosupports is an important factor to retain their efficient leaching and restrained redeposition with small sizes.

CONCLUSION

In summary, the framework of 3D-dendritic MSNSs have been demonstrated to be a desired colloidal nanosupport for catalysis. 3D-dendritic MSNSs have uniform particle size of ~125 nm with excellent monodispersity, center-radial pore channels with relatively short length of ~60 nm and large diameter of ~6 nm, and the amino groups can be functionalized on the inner silica wall surface of the mesopore channels via postgrafting approach with the well-preserved mesostructure. The ultradispersed palladium nanoparticles can be immobilized in amino-MSNSs with homogeneous distribution via an *in situ* growth strategy, because of their promoted accessibility of mesopore channels and mass-transport of reactants. Temperature plays the key role in controlling the sizes and uniformity of Pd nanoparticles in the *in situ* growth process, because the reducibility and coordination ability of amino group can be influenced with different temperatures. It is revealed that neither a high nor low reaction temperature is beneficial to homogeneous nucleation of palladium precursor, whereas the optimized condition is 30 °C, and Pd nanoparticles with a uniform small size of ~1.2 nm can be obtained. For Suzuki–Miyaura cross-coupling reactions, the 3D-dendritic MSNSs-based nanoreactors exhibit a high activity to various substrates, including electron-rich or electron-deficient ones. More importantly, the excellent reusability has been revealed in a recycling catalytic procedure, suggesting that the unique mesostructure of 3D-dendritic MSNSs can provide individual quasi-confined nanospaces to prevent aggregation of Pd nanoparticles. Thus, the 3D-dendritic MSNSs with the mesopore channels of short length and large diameter are supposed to be the desired nanosupports that can optimize mass-transport of reactants and pore accessibility. Moreover, they also can be used as supports for some other large-sized catalysts, especially enzyme molecules, and they would have more hopeful prospects in catalytic applications.

ASSOCIATED CONTENT

Supporting Information

TEM images of the samples extracted 3D-dendritic MSNS, Pd-MSNSs-10 and Pd-MSNSs-70, and Au-MSNSs; nitrogen adsorption–desorption isotherms, pore size distribution, FTIR spectra and SAXS patterns of the samples extracted 3D-dendritic MSNSs and amino-MSNSs; photo and XPS spectroscopy analysis of the samples Pd-MSNSs. The Supporting Information is available free of charge on the ACS Publications website at DOI: 10.1021/acsami.5b04992.

■ AUTHOR INFORMATION

Corresponding Author

*D. Zhao. E-mail: dzyzhao@fudan.edu.cn.

Notes

The authors declare the following competing financial interest(s): We reject Prof. Jean Marie Basset from KAUST Catalysis Center (KCC), King Abdullah University of Science and Technology, Thuwal (KSA) as a reviewer, for conflict of interest.

■ ACKNOWLEDGMENTS

The work was supported by China National Key Basic Research Program (973 Project) (2013CB934104, 2012CB224805), the NSFC (21210004), China Postdoctoral Science Foundation (2013M531113), Qatar University startup grant # QUSG-CAS-MST-14\15-1, and the authors extend their sincere appreciation to the Deanship of Scientific Research at King Saud University for its funding the Prolific Research group (PRG-1436-14).

■ REFERENCES

- (1) Bayne, L.; Ulijn, R. V.; Halling, P. J. Effect of Pore Size on The Performance of Immobilised Enzymes. *Chem. Soc. Rev.* **2013**, *42*, 9000–9010.
- (2) Bommarius, A. S.; Paye, M. F. Stabilizing Biocatalysts. *Chem. Soc. Rev.* **2013**, *42*, 6534–6565.
- (3) Perez-Lorenzo, M.; Vaz, B.; Salgueirino, V.; Correa-Duarte, M. A. Hollow-Shelled Nanoreactors Endowed with High Catalytic Activity. *Chem. - Eur. J.* **2013**, *19*, 12196–12211.
- (4) Torres Galvis, H. M.; de Jong, K. P. Catalysts for Production of Lower Olefins from Synthesis Gas: A Review. *ACS Catal.* **2013**, *3*, 2130–2149.
- (5) Deraedt, C.; Astruc, D. "Homeopathic" Palladium Nanoparticle Catalysis of Cross Carbon-Carbon Coupling Reactions. *Acc. Chem. Res.* **2014**, *47*, 494–503.
- (6) Liu, Y. P.; Chung, J.; Jang, Y.; Mao, S.; Kim, B. M.; Wang, Y. Q.; Guo, X. H. Magnetically Recoverable Nanoflake-Shaped Iron Oxide/Pt Heterogeneous Catalysts and Their Excellent Catalytic Performance in the Hydrogenation Reaction. *ACS Appl. Mater. Interfaces* **2014**, *6*, 1887–1892.
- (7) Ma, Z.; Dai, S. Design of Novel Structured Gold Nanocatalysts. *ACS Catal.* **2011**, *1*, 805–818.
- (8) Sun, Z. K.; Sun, B.; Qiao, M. H.; Wei, J.; Yue, Q.; Wang, C.; Deng, Y. H.; Kaliaguine, S.; Zhao, D. Y. A General Chelate-Assisted Co-Assembly to Metallic Nanoparticles-Incorporated Ordered Mesoporous Carbon Catalysts for Fischer–Tropsch Synthesis. *J. Am. Chem. Soc.* **2012**, *134*, 17653–17660.
- (9) Fang, X. L.; Liu, Z. H.; Hsieh, M. F.; Chen, M.; Liu, P. X.; Chen, C.; Zheng, N. F. Hollow Mesoporous Aluminosilica Spheres with Perpendicular Pore Channels as Catalytic Nanoreactors. *ACS Nano* **2012**, *6*, 4434–4444.
- (10) Zhang, Q.; Lee, I.; Joo, J. B.; Zaera, F.; Yin, Y. Core-Shell Nanostructured Catalysts. *Acc. Chem. Res.* **2012**, *46*, 1816–1824.
- (11) Diaz, U.; Brunel, D.; Corma, A. Catalysis Using Multifunctional Organosiliceous Hybrid Materials. *Chem. Soc. Rev.* **2013**, *42*, 4083–4097.
- (12) Li, W.; Yue, Q.; Deng, Y. H.; Zhao, D. Y. Ordered Mesoporous Materials Based on Interfacial Assembly and Engineering. *Adv. Mater.* **2013**, *25*, 5129–5152.
- (13) Lu, G.; Li, S. Z.; Guo, Z.; Farha, O. K.; Hauser, B. G.; Qi, X. Y.; Wang, Y.; Wang, X.; Han, S. Y.; Liu, X. G.; DuChene, J. S.; Zhang, H.; Zhang, Q. C.; Chen, X. D.; Ma, J.; Loo, S. C. J.; Wei, W. D.; Yang, Y. H.; Hupp, J. T.; Huo, F. W. Imparting functionality to a metal-organic framework material by controlled nanoparticle encapsulation. *Nat. Chem.* **2012**, *4*, 310–316.
- (14) Zhu, Q. L.; Li, J.; Xu, Q. Immobilizing Metal Nanoparticles to Metal-Organic Frameworks with Size and Location Control for Optimizing Catalytic Performance. *J. Am. Chem. Soc.* **2013**, *135*, 10210–10213.
- (15) Wang, S.; Zhao, Q. F.; Wei, H. M.; Wang, J. Q.; Cho, M. Y.; Cho, H. S.; Terasaki, O.; Wan, Y. Aggregation-Free Gold Nanoparticles in Ordered Mesoporous Carbons: Toward Highly Active and Stable Heterogeneous Catalysts. *J. Am. Chem. Soc.* **2013**, *135*, 11849–11860.
- (16) Prieto, G.; Shakeri, M.; de Jong, K. P.; de Jongh, P. E. Quantitative Relationship between Support Porosity and the Stability of Pore-confined Metal Nanoparticles Studied on CuZnO/SiO₂-Methanol Synthesis Catalysts. *ACS Nano* **2014**, *8*, 2522–2531.
- (17) Yue, Q.; Wang, M. H.; Wei, J.; Deng, Y. H.; Liu, T. Y.; Che, R. C.; Tu, B.; Zhao, D. Y. A Template Carbonization Strategy to Synthesize Ordered Mesoporous Silica Microspheres with Trapped Sulfonated Carbon Nanoparticles for Efficient Catalysis. *Angew. Chem., Int. Ed.* **2012**, *51*, 10368–10372.
- (18) Zurner, A.; Kirstein, J.; Dobliger, M.; Brauchle, C.; Bein, T. Visualizing Single-molecule Diffusion in Mesoporous Materials. *Nature* **2007**, *450*, 705–708.
- (19) Karger, J.; Valiullin, R. Mass Transfer in Mesoporous Materials: the Benefit of Microscopic Diffusion Measurement. *Chem. Soc. Rev.* **2013**, *42*, 4172–4197.
- (20) Zhao, D.; Feng, J.; Huo, Q.; Melosh, N.; Fredrickson, G. H.; Chmelka, B. F.; Stucky, G. D. Triblock Copolymer Syntheses of Mesoporous Silica with Periodic 50 to 300 Angstrom Pores. *Science* **1998**, *279*, 548–552.
- (21) Pirez, C.; Caderon, J. M.; Dacquin, J. P.; Lee, A. F.; Wilson, K. Tunable KIT-6 Mesoporous Sulfonic Acid Catalysts for Fatty Acid Esterification. *ACS Catal.* **2012**, *2*, 1607–1614.
- (22) Parlett, C. M. A.; Bruce, D. W.; Hondow, N. S.; Lee, A. F.; Wilson, K. Support-Enhanced Selective Aerobic Alcohol Oxidation over Pd/Mesoporous Silicas. *ACS Catal.* **2011**, *1*, 636–640.
- (23) Yepez, A.; Hidalgo, J. M.; Pineda, A.; Cerny, R.; Jisa, P.; Garcia, A.; Romero, A. A.; Luque, R. Mechanistic Insights Into The Hydroconversion of Cinnamaldehyde Using Mechanochemically-synthesized Pd/Al-SBA-15 Catalysts. *Green Chem.* **2015**, *17*, 565–572.
- (24) Engstrom, K.; Johnston, E. V.; Verho, O.; Gustafson, K. P. J.; Shakeri, M.; Tai, C.-W.; Backvall, J.-E. Co-immobilization of an Enzyme and a Metal into the Compartments of Mesoporous Silica for Cooperative Tandem Catalysis: An Artificial Metalloenzyme. *Angew. Chem., Int. Ed.* **2013**, *52*, 14006–14010.
- (25) Joo, S. H.; Park, J. Y.; Tsung, C.-K.; Yamada, Y.; Yang, P.; Somorjai, G. A. Thermally Stable Pt/mesoporous Silica Core-shell Nanocatalysts for High-temperature Reactions. *Nat. Mater.* **2009**, *8*, 126–131.
- (26) Zhang, W.; Wang, S.; Zhang, M. Yolk-Shell Catalyst of Single Au Nanoparticle Encapsulated within Hollow Mesoporous Silica Microspheres. *ACS Catal.* **2011**, *1*, 207–211.
- (27) Sun, Z.; Yang, J.; Wang, J.; Li, W.; Kaliaguine, S.; Hou, X.; Deng, Y.; Zhao, D. A Versatile Designed Synthesis of Magnetically Separable Nano-catalysts with Well-defined Core-shell Nanostructures. *J. Mater. Chem. A* **2014**, *2*, 6071–6074.
- (28) Liu, W. J.; Zhu, Z. N.; Deng, K.; Li, Z. T.; Zhou, Y. L.; Qu, H. B.; Gao, Y.; Che, S. N.; Tang, Z. Y. Gold Nanorod@Chiral Mesoporous Silica Core-shell Nanoparticles with Unique Optical Properties. *J. Am. Chem. Soc.* **2013**, *135*, 9659–9664.
- (29) Tan, L. F.; Chen, D.; Liu, H. Y.; Tang, F. Q. A Silica Nanorattle with a Mesoporous Shell: An Ideal Nanoreactor for the Preparation of Tunable Gold Cores. *Adv. Mater.* **2010**, *22*, 4885–4889.
- (30) Zhang, K.; Chen, H. R.; Zhou, X. X.; Gong, Y.; Zhang, G. B.; Wang, X.; Chen, Y.; Shi, J. L. Unconventional Pd Nanoparticles' Growth Induced by a Competitive Effect Between Temperature-dependent Coordination and Reduction of Grafted Amino Ligands for Heck Reaction. *J. Mater. Chem. A* **2014**, *2*, 1515–1523.
- (31) Shen, D. K.; Yang, J. P.; Li, X. M.; Zhou, L.; Zhang, R. Y.; Li, W.; Chen, L.; Wang, R.; Zhang, F.; Zhao, D. Y. Biphasic Stratification

Approach to Three-Dimensional Dendritic Biodegradable Mesoporous Silica Nanospheres. *Nano Lett.* **2014**, *14*, 923–932.

(32) Collins, G.; Schmidt, M.; O'Dwyer, C.; McGlacken, G.; Holmes, J. D. Enhanced Catalytic Activity of High-Index Faceted Palladium Nanoparticles in Suzuki Miyaura Coupling Due to Efficient Leaching Mechanism. *ACS Catal.* **2014**, *4*, 3105–3111.

(33) Perez-Lorenzo, M. Palladium Nanoparticles as Efficient Catalysts for Suzuki Cross-Coupling Reactions. *J. Phys. Chem. Lett.* **2012**, *3*, 167–174.

(34) Balanta, A.; Godard, C.; Claver, C. Pd Nanoparticles for C-C Coupling Reactions. *Chem. Soc. Rev.* **2011**, *40*, 4973–4985.

(35) Fihri, A.; Bouhrara, M.; Nekoueishahraki, B.; Basset, J. M.; Polshettiwar, V. Nanocatalysts for Suzuki Cross-coupling Reactions. *Chem. Soc. Rev.* **2011**, *40*, 5181–5203.

(36) Molnar, A. Efficient, Selective, and Recyclable Palladium Catalysts in Carbon-Carbon Coupling Reactions. *Chem. Rev.* **2011**, *111*, 2251–2320.

(37) Scheuermann, G. M.; Rumi, L.; Steurer, P.; Bannwarth, W.; Mulhaupt, R. Palladium Nanoparticles on Graphite Oxide and Its Functionalized Graphene Derivatives as Highly Active Catalysts for the Suzuki-Miyaura Coupling Reaction. *J. Am. Chem. Soc.* **2009**, *131*, 8262–8270.